

Testing Dirac-Brueckner models in collective flow of heavy-ion collisions

T. Gaitanos¹, C. Fuchs², H.H. Wolter¹, and Amand Faessler²

¹ *Sektion Physik der Universität München, Am Coulombwall 1, D-85748 Garching, Germany*

² *Institut für Theoretische Physik der Universität Tübingen, Auf der Morgenstelle 14, D-72076 Tübingen, Germany*

We investigate differential in-plane and out-of-plane flow observables in heavy ion reactions at intermediate energies from $0.2 \div 2$ AGeV within the framework of relativistic BUU transport calculations. The mean field is based on microscopic Dirac-Brueckner-Hartree-Fock (DBHF) calculations. We apply two different sets of DBHF predictions, those of ter Haar and Malfliet and more recent ones from the Tübingen group. Both models show similar trends but differ in details. The latter DBHF calculations exclude thereby spurious contributions from the negative energy sector to the mean field which results in a slightly softer equation of state and a less repulsive momentum dependence of the nucleon-nucleus potential at high densities and high momenta. For the application to heavy ion collisions in both cases non-equilibrium features of the phase space are taken into account on the level of the effective interaction. The systematic comparison to experimental data favours the less repulsive and softer model. Compared to non-relativistic approaches here larger values of the effective in-medium nucleon mass produce already a sufficient amount of repulsion to describe the differential flow data reasonably well.

I. INTRODUCTION

Relativistic heavy-ion collisions have been extensively investigated to determine the nuclear equation-of-state (EOS) far away from saturation and at finite temperature, using semi-classical transport models of the Boltzmann-type [1,2]. The nuclear EOS which enters into a transport description via density and momentum dependent mean fields has mostly been based on phenomenological considerations by adjusting the parameters to nuclear matter saturation properties and to the momentum dependence of the empirical nucleon-nucleus optical potential [3]. Such parametrisations, as e.g. Skyrme-type potentials [4], imply different extrapolations to high and low densities and high momenta, which should be tested in heavy ion reactions. Thus there have been many efforts to determine the density and momentum dependence of the nuclear mean field by studying the different aspects of the collective flow in intermediate energy heavy ion collisions between $0.1 - 2$ AGeV (SIS-energies) [4–12].

On the other hand, it is well known that hadrons generally change their properties in the medium. This basic feature is already incorporated in the simplest version of a relativistic hadronic model for nuclear matter, namely linear Quantum Hadron Dynamics (QHD) [13], where the effective nucleon mass drops with density. To obtain a reasonable compressibility scalar self-interaction

terms are introduced and finite nuclei are well described [14]. At much higher densities, i.e. for the description of neutron stars, also non-linear terms of the vector mean field are required [15]. These different treatments reflect the inherent uncertainties in density extrapolations away from the saturation point. More recent and systematic approaches try to fix the relevant terms, e.g. by density functional expansions of generalised QHD lagrangians [16,17] which effectively incorporate the basic features of chiral symmetry and its breaking. However, predictions for high densities remain questionable since effective field theory provides a low density expansion scheme valid in the vicinity of the nuclear saturation point and below [17,18].

An alternative approach to the density and momentum dependence of the mean field is provided by microscopic many-body models. Here the nucleon-nucleon (NN) interaction is fixed by free NN-scattering and no parameters are adjusted to the nuclear matter problem. In the relativistic Dirac-Brueckner-Hartree-Fock (DB) approach [19–24] the NN-interaction is based on modern one-boson-exchange (OBE) potentials [25] and the in-medium ladder diagrams are summed self-consistently. Although not perfectly, this approach describes the nuclear matter saturation properties reasonably, which is not trivial since a corresponding self-consistent Hartree-Fock calculation without higher order correlations does not even lead to a saturation of nuclear matter. Then the success of non-linear QHD lagrangians can be interpreted in that these models phenomenologically parametrise the density dependence of the microscopic DB predictions [26]. However, the constraints from finite nuclei on the explicit form of the fields are limited since the single particle potential results from the cancellation of large scalar and vector potentials. Only the spin-orbit interaction allows to constrain the magnitude of the effective mass [14,16,24]. On the other hand, in energetic heavy ion reactions scalar and vector fields are decoupled by their different Lorentz transformation properties, in the sense that they can be tested independently, and additional information on the structure of the potential can be obtained. Thus within the DB framework there is the chance to attempt a *unified* description of different nuclear systems, i.e. free NN-scattering, nuclear matter, finite nuclei and heavy ion collision.

However, relativistic Brueckner calculations are not straightforward and the approaches of various groups [20–23] are similar but differ in detail, depending on solution techniques and the particular approximations made. In the present work we therefore want to study in heavy

ion collisions at intermediate energies DB prediction for the density and momentum dependence of the nuclear mean field in more detail. In previous studies [11,12] a qualitative agreement with collective flow observables has been found. Recently more detailed experiments have been performed for differential components of the collective flow [27]. In particular, the rapidity and transverse momentum dependence of collective flow has attracted much theoretical interest because of their strong sensitivity to the momentum dependence of the nuclear mean field [9]. Here we test the self energies, i.e. the nuclear EOS, from two different DB calculations, from ter Haar and Malfliet [21] and from a more recent study performed by the Tübingen group [22,23].

In heavy ion collisions a further difficulty arises due to the non-equilibrium features of the phase space configurations. This has been discussed before in ref. [11,12]. In a fully consistent treatment, one would have to solve the coupled set of DB equations for the effective interaction in non-equilibrium nuclear matter configurations simultaneously with the kinetic equations for the evolution of a phase space distribution [20]. However, such a procedure has not been realized yet, and further approximations are necessary in heavy ion collisions. In the local density approximation (LDA) the nuclear matter mean fields are directly used in the transport calculation. However, this approximation is not reliable enough at intermediate energies, because the local momentum space is highly anisotropic during a large part of the heavy ion collision [12,28,29]. A better approximation is the colliding nuclear matter (CNM) approach, where the phase space anisotropies are parametrised by two inter-penetrating nuclear matter currents, i.e. the local momentum space is given by two Fermi-spheres, or covariant Fermi-ellipsoids, with given Fermi momenta and a relative velocity [30]. In Ref. [30] a method was developed to extrapolate nuclear matter DB results to CNM configurations. The CNM self energies are applied to heavy ion collisions in the Local (phase space) Configuration Approximation (LCA) [11,12,31], where the anisotropic phase space is locally parametrised by a CNM configuration. In this paper the LCA approximation is only briefly discussed, details can be found in [11,12,30]. We shall discuss the density and momentum dependence of the DB mean fields and their application to the CNM approximation in terms of an effective equation of state [32].

This paper is organised as follows: In section IV the transport equation and their numerical realization is outlined. Then we discuss the density and momentum dependence of the DB mean fields in ground state nuclear matter, and the LCA approximation for anisotropic phase space configurations in heavy ion collisions. Section V contains the results of transport calculations based on the DB mean fields of Refs. [21,23] in the LCA approximation. We compare different components of collective flow with respect to its energy, centrality, transverse momentum and rapidity dependence. It is found that both models are able to qualitatively describe the experimen-

tal results, but in details one finds model dependences on the collective flow observables.

II. THE DB APPROACH

Brueckner theory provides a microscopic model which accounts for two-body correlations in the ladder approximation in medium in the Bethe-Goldstone or the Bethe-Salpeter equation in the relativistic case,

$$\mathcal{T} = V + i \int VGGT \quad . \quad (1)$$

The correlations of the Green functions, or wave functions respectively, are shifted to the effective in-medium interaction, i.e. the \mathcal{T} -matrix (or \mathcal{G} -matrix) [20]. The in-medium propagator obeys a Dyson equation

$$G = G^0 + \int G^0 \Sigma G \quad (2)$$

and is dressed by a self-energy Σ obtained in Hartree-Fock approximation from the \mathcal{T} -matrix

$$\Sigma = -i \int \mathcal{T}G \quad . \quad (3)$$

The coupled set of equations (1-3) has to be solved self-consistently. In this procedure the bare interaction V , iterated in the Bethe-Salpeter equation, is sandwiched between dressed in-medium spinors. This feature is absent in non-relativistic approaches and introduces an additional density dependence which is responsible for the significantly improved saturations properties compared to non-relativistic \mathcal{G} -matrix calculations [38,39]. The non-relativistic Brueckner approach leads to too large saturation densities (e.g. $\rho_{\text{sat}} = 0.2 \text{ fm}^{-3}$ in [38] and $\rho_{\text{sat}} = 0.24 \text{ fm}^{-3}$ in [39]) and predicts a rather small compressibility ($K=180 \text{ MeV}$ in [31,38]). The introduction of 3-body-forces can in principle improve on this in the non-relativistic case [39].

In contrast to the phenomenological approaches like QHD [13] and to effective field theory [16,18] this approach is essentially parameter free. The only free parameters are those of the NN-interaction, namely those of the realistic OBE potentials, which are fixed by the free scattering problem [25]. The success of the DB model indicates that it already accounts for the most important set of diagrams to describe nuclear matter. A further inclusion of particle-hole correlations around the DB mean field also can ensure thermodynamical consistency in the form of the Hugenholtz-van-Hove theorem [40,41].

In the present work we employ the results of two different DB calculations, those of Ref. [21] and the more recent ones of Ref. [23], denoted as DBHM and DBT, respectively, in the following. We will briefly characterise the difference between these two calculations. One difference is the use of different OBE potentials; in [21] a

version of the Groningen potential and in [23] the Bonn A potential. In both cases the same set of six non-strange mesons with masses below 1 GeV is used and the fit to the NN phase shifts is of similar quality, however, the actual model parameters (coupling constants and form factors) are different. The main difference between these two approaches has, however, a more complicated origin, which is discussed in detail in [22,23]. The DB structure equations (1-3) are matrix equations in spinor space. To determine the Dirac structure of the self energy, i.e. the scalar (Σ_s) and a vector (Σ^μ) contributions,

$$\Sigma_{\alpha\beta} = \mathbb{1}_{\alpha\beta}\Sigma_s - \gamma^\mu_{\alpha\beta}\Sigma_\mu \quad (4)$$

the \mathcal{T} -matrix has to be decomposed into its Lorentz components, i.e. scalar, vector, tensor, etc. contributions. This procedure is not free from ambiguities. Due to identical matrix elements for positive energy states pseudo-scalar and pseudo-vector components cannot uniquely be disentangled for the on-shell \mathcal{T} -matrix. However, with a pseudo-scalar vertex the pion couples maximally to negative energy states which are not included in the standard Brueckner approach. This is inconsistent with the potentials used since the OBE potentials are also based on the no-sea approximation. Hence, pseudo-scalar contributions due to the 1- π exchange lead to large and spurious contributions from negative energy states. In [22] it was shown that such spurious contributions dominate the momentum dependence of the nuclear self-energy, and, in particular, lead to an artificially strong momentum dependence inside the Fermi sea. It was further demonstrated in [22] that the method used in [21] fails to cure this problem and in [23] a new and reliable method was proposed to remove those spurious contributions from the \mathcal{T} -matrix.

The saturation properties of the two DB calculations are given in Table 1. It is seen there that the results of ter Haar and Malfliet (DBHM) [21] give a slightly better saturation density compared to [23] (DBT) but too little binding. DBT, in contrast, gives a good binding energy and also meets the empirical range of saturation. The stiffness of the EOS expressed by the compression modulus is similar for both approaches. A significant difference can be observed for the magnitude of the effective mass but both values are still consistent with the knowledge from finite nuclei on the strength of the spin-orbit force ($500 \text{ MeV} \leq m^* \leq 700 \text{ MeV}$) [17].

TABLE I. Saturation properties of nuclear matter, i.e. Fermi-momentum k_F , saturation density ρ_{sat} , binding energy per particle E/A , effective mass m^* and the compression modulus K in the DBHF calculations of [21] (DBHM) and [23] (DBT).

	k_F [fm $^{-1}$]	ρ_{sat} [fm $^{-3}$]	E/A [MeV]	m^* [MeV]	K [MeV]
DBHM	1.343	0.164	-13.6	558	250
DBT	1.39	0.185	-16.1	637	230

We also note that the relativistic effective mass, i.e. the Dirac mass $m^* = M - \Sigma_s$ given in Table 1, should be distinguished from the effective mass m_{NR}^* which in non-relativistic approaches is used to classify the non-locality of the mean field [9,10]. The latter is defined by

$$m_{NR}^* = |\mathbf{k}| \left(\frac{\partial k^0}{\partial |\mathbf{k}|} \right)^{-1} \quad (5)$$

and is approximately $m_{NR}^* \approx k_0^* = \sqrt{\mathbf{k}^2 + m^{*2}}$. At ρ_0 the two models DBHM/DBT yield the following values $m_{NR}^*(k_F)/M = 0.63/0.73$ which can be compared to the parameters used in refs. [9,10].

The corresponding equations-of-state are shown in Fig.1 as a function of the baryon density ρ . Both EOSs are quite similar up to about $2\rho_0$ where the softer character of the DBT becomes more pronounced.

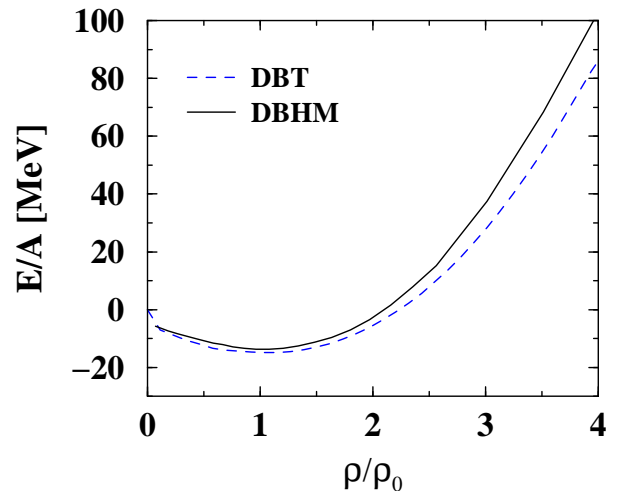


FIG. 1. Equation of states in the DB approaches. Solid: DB calculations from [21], dashed: DB calculations from [23].

Fig.2 shows the density dependence of the mean field. Both calculations show an almost linear increase of the vector self-energy Σ_0 with density, but for Σ_s DBHM shows a more non-linear behaviour than DBT. In the DBT approach the fields are generally smaller by about 50-100 MeV compared to DBHM. The same trend can be seen from Fig.3 where the momentum dependence of the scalar and vector potentials at densities ρ_0 , $2\rho_0$ and $3\rho_0$ is shown. In both calculations scalar and vector fields decrease with increasing momentum in a similar way. Generally, the explicit momentum dependence is moderate at densities $\rho \leq \rho_0$ but becomes pronounced at higher densities. In ref. [21] constant values of Σ are taken for momenta below the Fermi momentum whereas the results of [23] reflect the full momentum dependence outside and inside the Fermi sea. The difference in the magnitude of the fields Σ_s and Σ_0 in the two approaches can be traced back to the different projection schemes discussed above. With the correct and complete pseudo-vector description for the pion contributions the fields

are dominated by the σ and ω contributions and the other mesons π (pseudo-vector coupling), ρ , η , δ give only small corrections [22,23]. However, with the method used in [21] large, but spurious contributions from a pseudo-scalar pion-exchange lead to an additional enhancement of both, scalar and vector fields seen in Figs. 2 and 3.

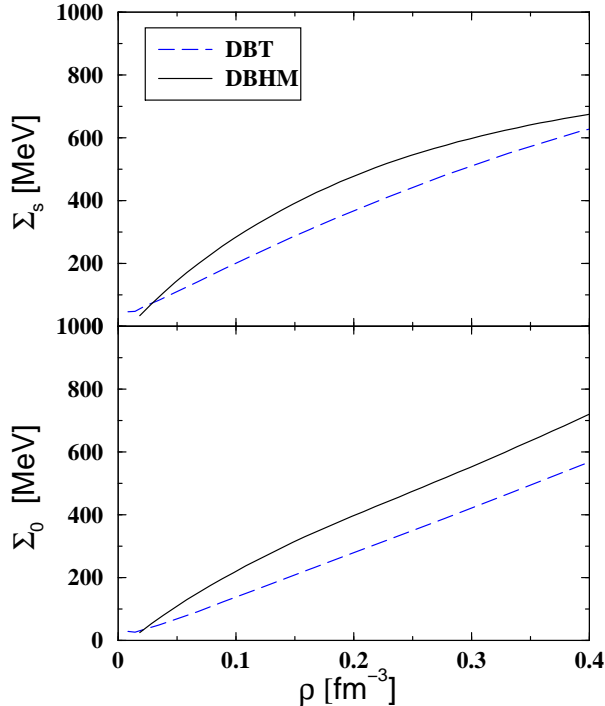


FIG. 2. Scalar (top) and vector (bottom) self energies as in Fig. 1

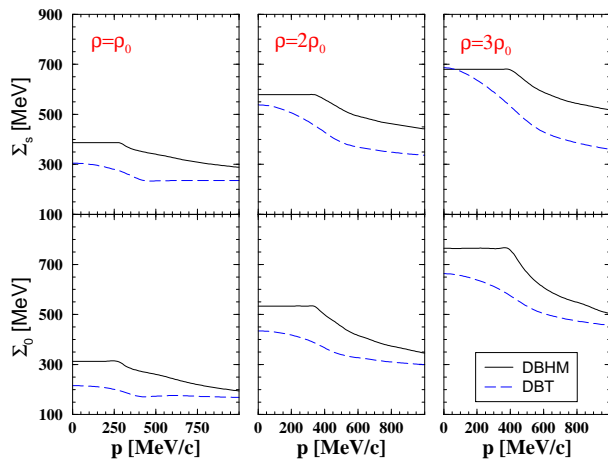


FIG. 3. Momentum dependence of the scalar (top) and vector (bottom) self energies at $\rho = 1/2/3\rho_0$. The solid lines are DB calculations from [21] and the dashed curves from [23].

Fig.4 shows the real part of the optical Schroedinger-equivalent nucleon potential, defined as

$$U_{\text{opt}} = -\Sigma_s + \frac{k^0}{M}\Sigma_0 + \frac{\Sigma_s^2 - \Sigma_\mu^2}{2M}, \quad (6)$$

in nuclear matter as a function of its laboratory energy $E_{\text{lab}} = k^0 - M$. Note that the definition of an optical potential is not unique in the literature, e.g. in refs. [9,42] an optical potential is defined as the difference of the single-particle energies in the medium and in free space $U = k^0 - \sqrt{M^2 + \mathbf{k}^2}$. The optical potential defined by Eq. (6) is the Schroedinger-equivalent relativistic potential [21] and can be covariantly defined by $U_{\text{opt}} = (k_\mu^2 - M^2)/2M = ((k_\mu^* + \Sigma_\mu)^2 - M^2)/2M$ which is obviously a Lorentz scalar.

As can be seen from Eq. (6) a momentum independent vector potential Σ_0 (as in the mean field approximation of QHD) leads to a linear energy dependence of the optical potential, i.e. a momentum dependence $\frac{\Sigma_0(\rho)}{2M^2}p^2$. The explicit momentum dependence of the DB fields asymptotically is $\Sigma_{0,S} \sim (A+B/p)$ which still leads to a linear increase of U_{opt} at large energies. As seen in Fig. 4 the empirical optical potential [3] extracted from proton-nucleus scattering for nuclear matter at ρ_0 is reasonably well reproduced up to an energy of about 600-800 MeV. However, it shows a saturation behaviour at large momenta which cannot be reproduced by DB calculations. It was found that in heavy ion reactions at incident energies above 1 AGeV such a saturation behaviour is required to reproduce transverse flow observables [8]. Thus, DB mean fields start to become unrealistic above 1 AGeV. There exist presently no microscopic calculations which are able to reproduce this saturation behaviour of the optical potential. Therefore we restrict our investigation of transverse flow observables to an energy range where the DB fields can be safely applied. At higher energies one has to rely on phenomenological approaches where the strength of the vector potential is artificially suppressed, e.g. by the introduction of additional form factors [8].

One should be aware that the empirical optical potential involves densities around ρ_0 and does not completely constrain the mean fields that enter in a heavy ion collision, which involve large values of momentum and density. As a common feature relativistic DB calculation show a strong and repulsive momentum dependence also at high densities [21,23,42] whereas, e.g. the non-relativistic \mathcal{G} -matrix of ref. [39] has a much less repulsive high density behaviour. In first order the strength of the repulsion in the relativistic case is determined by the magnitude of the vector field. As can be seen from Fig.4 the two approaches DBHM and DBT yield similar results at moderate densities $\rho \leq \rho_0$ but differences become substantial at high densities. The generally smaller fields of DBT result in a less repulsive potential at high densities. The test of DB fields in heavy ion collisions where high densities and momenta greater than the Fermi-momentum ($\rho \approx 2 - 3\rho_0$) can be reached, should allow to differentiate between the DB models.

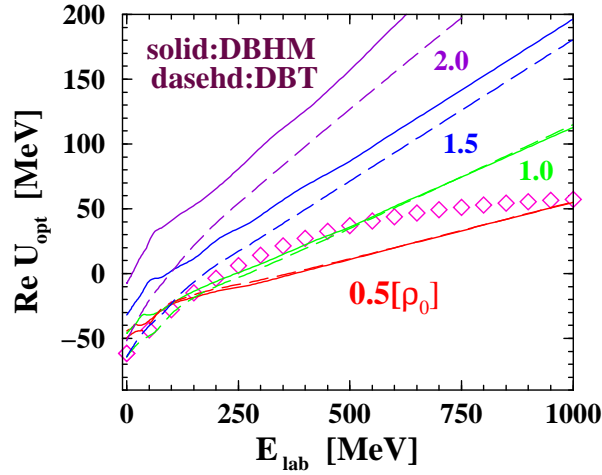


FIG. 4. Same as in Fig. 1 for the energy dependence of the optical potential.

III. THE CNM APPROXIMATION

The DB approach discussed in the previous section describes equilibrated nuclear matter which is characterised by one Fermi-sphere of a given Fermi-momentum. In a local density approximation (LDA) these self energies are directly inserted into the drift term of the RBUU equation. However, as discussed before, local momentum space anisotropies are a characteristic feature of energetic heavy ion reactions. The time scales where such anisotropies occur are comparable with the compression phase of the process [12,28,29]. It was found that the local anisotropic momentum space can well be parametrised by two inter-penetrating nuclear matter currents, i.e. by two Fermi-spheres in momentum space [28,29], or the Colliding Nuclear Matter (CNM) [30] which is schematically illustrated in Fig.5. The application of the DB model to CNM configurations has, however, not been realized yet relativistically, but only in non-relativistic \mathcal{G} -matrix calculations [38].

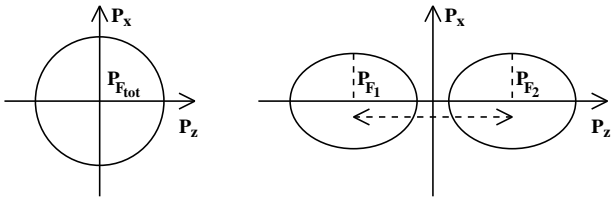


FIG. 5. Schematic representation of the LDA (nuclear matter) and LCA (colliding nuclear matter) approximations.

Therefore in Ref. [30] a method was developed to extrapolate DB results to such CNM configurations. We summarise the main features of this approach.

The CNM momentum distribution is constructed by a superposition of the single currents, i.e.

$$f_{12}(\mathbf{k}^*) = f_1(\mathbf{k}^*) + f_2(\mathbf{k}^*) + \delta f \\ = \Theta(k_{F_1} - k_{\mu}^* u_1^{\mu}) + \Theta(k_{F_2} - k_{\mu}^* u_2^{\mu}) + \delta f \quad , \quad (7)$$

where f_i are the covariant momentum space distributions of the two NM currents and $\delta f = -f_1 f_2$ is a correction term which takes into account Pauli-blocking effects in the overlap region of the two nuclear matter currents. The corresponding CNM self energies $\Sigma_{s,0}(k; \chi)$ depend explicitly on momentum and the configuration parameters $\chi \equiv \{k_{F_1}, k_{F_2}, v_{rel}\}$ (Fermi-momenta $k_{F_{1,2}}$ and the relative velocity v_{rel}). Averaging the CNM configuration, Eq. (7), over momentum leads to mean self energies which depend only on the parameters of the CNM momentum space distributions.

The consideration of anisotropy effects in the CNM approximation leads to non-equilibrium mean fields, which essentially differ from those of the equilibrium case. In analogy to the non-equilibrium self energies we construct a non-equilibrium EOS [30], i.e. an equation of state which depends on the CNM parameters. However, the total energy of the CNM system includes the kinetic energy of the relative motion of the two nuclear matter currents. In order to compare with the compression energy one should subtract this kinetic (and repulsive) component from the total energy which yields the “reduced” binding energy E_{12}^{bind} of the CNM system. The limiting case of $v_{rel} \rightarrow 0$ the equilibrium EOS is recovered. Fig.6 shows the EOS’s for different symmetric ($k_F \equiv k_{F_1} = k_{F_2}$) CNM configurations. It is seen in both models that the effective non-equilibrium EOS is softer compared to the equilibrium EOS (solid curves for vanishing relative velocity). However, the different density and momentum dependence of the two DB models leads to a different magnitude of this softening effect, in particular with increasing relative velocity.

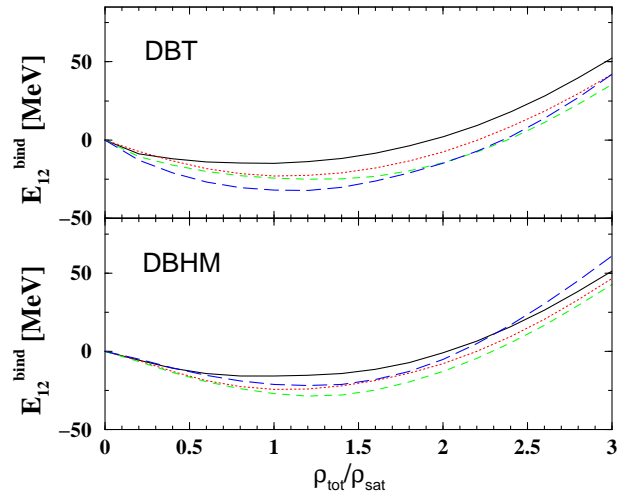


FIG. 6. Reduced EOS’s for the CNM approximation using the DB results of Ref. [21] (top) and [23] (bottom). The Different curves give the CNM EOS’s for different relative velocities ($v_{rel} = 0, 0.2, 0.4, 0.6$ for solid, dotted, dashed and long-dashed curves, respectively).

The reason for this softening of the effective EOS in colliding nuclear matter is the fact that in the participant zone of the reaction particles which belong to projectile and target are separated in momentum space. This simple geometrical effect works similar as an additional virtual new degree of freedom and leads to a softening of the effective EOS experienced by the nucleons in such configurations. This type of phase space effect is not included in standard transport calculations for heavy ion collisions, even when momentum dependent interactions are used [9,10]. Phenomenological mean fields $U(\mathbf{x}, \mathbf{k}) = U_{\text{loc}}(\varrho(\mathbf{x})) + U_{\text{nonloc}}(\mathbf{x}, \mathbf{k})$ are usually composed by a local, density dependent potential $U_{\text{loc}}(\varrho(\mathbf{x}))$ and a non-local momentum dependent part $U_{\text{nonloc}}(\mathbf{x}, \mathbf{k}) = \int d^3k' f(\mathbf{x}, \mathbf{k}') V(\mathbf{x}, \mathbf{k} - \mathbf{k}')$ with V an effective momentum dependent two-body-interaction. Whereas $U_{\text{nonloc}}(\mathbf{x}, \mathbf{k})$ accounts properly for the actual momentum space configurations $f(\mathbf{x}, \mathbf{k}')$, the local part does not depend on the momentum space. Consequently, $U_{\text{loc}}(\varrho)$ reflects a density dependence which is correct in equilibrated nuclear matter but does not apply to anisotropic momentum space configurations.

IV. THE TRANSPORT MODEL

In the present work heavy ion collisions are treated by the relativistic (R)BUU equation [2,11,12]

$$\left\{ k_{\mu}^* \partial_x^{\mu} + [k_{\nu}^* F^{\mu\nu} + m^* (\partial_x^{\mu} m^*)] \partial_{\mu}^{k^*} \right\} f(x, k^*) = I_{\text{coll}} \quad . \quad (8)$$

This equation describes the evolution of a classical 1-body phase space distribution $f(x, k^*)$ under the influence of a self-consistent mean field, or the scalar and vector self energies Σ_s and Σ^{μ} . The self-energies determine effective momenta and masses of the dressed quasi-particles in the nuclear medium $k^{*\mu} = k^{\mu} - \Sigma^{\mu}$, $m^* = M - \Sigma_s$. The field strength tensor of the vector field $F^{\mu\nu} = \partial^{\mu} \Sigma^{\nu} - \partial^{\nu} \Sigma^{\mu}$ gives rise to a Lorentz force as in electrodynamics. This introduces in a most natural way a first order momentum dependence which in non-relativistic treatments has to be parameterised explicitly [1,4,7]. The collision term describes 2-body collisions and is treated by cascade-like Monte-Carlo simulations, as in relativistic versions of the QMD-model [37]. We include the relevant nucleonic excitations at SIS energies, i.e. the $\Delta(1232)$ and $N^*(1440)$ resonances and their decay to one- and two-pion states. The cross-sections for elastic and inelastic scattering as well as differential cross sections are taken from Ref. [33] which are used also in QMD calculations at SIS energies [34,35]. The drift term of the RBUU equation (8) is numerically treated in the relativistic Landau-Vlasov method (RLV) [36]. This is a test particle method, where the test particles are represented by manifestly covariant Gaussians in phase space. In order to reduce numerical fluctuations a number of

50 – 100 test particles per nucleon was found to be sufficient here. Energy-momentum conservation is fulfilled in our calculations with an accuracy of 3 – 5 % of the initial kinetic centre-of-mass energy of the colliding nuclei.

The anisotropic phase space effects discussed above are incorporated in heavy ion collisions by applying the CNM or non-equilibrium DB mean fields in the framework of a Local Configuration Approximation (LCA) [11,12,29]. In this approach the phase space is parametrised locally by a CNM configuration where the invariant configuration parameters χ are directly determined from the phase space distribution $f(x, k^*)$. Transport calculations have shown that the collective flow is reduced if the non-equilibrium effects are taken into account [12] which is consistent with a softening of the effective EOS in heavy ion collisions as discussed above. This will be investigated more systematically below.

V. COLLECTIVE FLOW EFFECTS

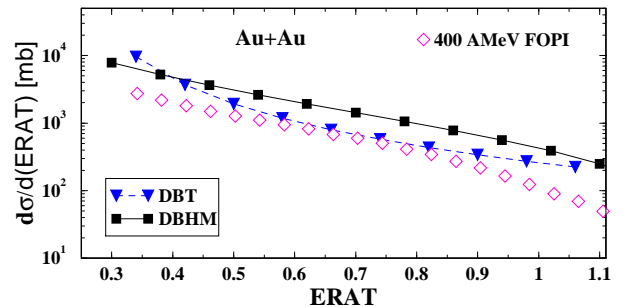


FIG. 7. $ERAT$ cross sections for Au+Au reactions at 0.4 AGeV beam energy. Transport calculations with the DB mean fields from Refs. [21] (DBHM) [23] (DBT) are compared with the FOPI data [44].

In this section different types of collective flow observables are investigated in transport calculations using the DBHM/DBT mean fields in the local phase space configuration approximation (LCA). To compare with experiments the same methods are used for centrality selection, and reaction plane determination, and the theoretical results are subjected to filter routines to simulate the experimental detector efficiencies, if necessary. Since we mainly compare to results from the FOPI Collaboration [6,27,44,45] these correspond to the FOPI (Phase-I or Phase-II) set up. These filters are sensitive to fragment distributions. Thus we also generate fragments in the final state of the reaction (at $\approx 100 - 200$ fm/c depending on the incident energy) using a phenomenological phase space coalescence model [12,46].

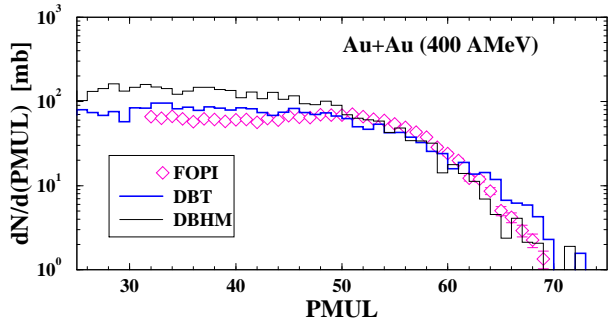


FIG. 8. Same as Fig. 7 for the multiplicity of charged particles.

Criteria for the determination of the centrality class of an event are the multiplicity of charged particles ($PMUL$) and/or the ratio of transversal to longitudinal energy ($ERAT$) [47]. As an example, in Figs.7 and 8 these observables are shown for an energy of 0.4 AGeV and compared to FOPI data [44,47]. Fig.7 displays the differential cross section $d\sigma/d(ERAT)$. Large $ERAT$ values correspond to central reactions whereas small values indicate semi-peripheral and peripheral reactions [12,44,47]. A qualitative agreement with experiment is achieved for both mean fields, with DBHM somewhat overestimating the data. Stronger stopping will result in flatter $d\sigma/d(ERAT)$ curve, and thus it is seen that DBHM shows generally more stopping, at least for peripheral to mid central collisions. This result will also be seen below from the rapidity distributions. At large $ERAT$ values for the most central collisions the theoretical predictions deviate from the measured cross sections.

In Fig.8 the multiplicity distributions $d\sigma/d(PMUL)$ are shown. Also here the agreement with experiment is reasonable for DBHM and quite good for DBT. Particularly, we can reproduce the plateau (in logarithmic scale) of these distributions which is used in the centrality selection. Altogether, the good agreement with experiment makes the centrality selection reliable using either the $PMUL$ or $ERAT$ observable. In the following we will apply mostly the $PMUL$ criterion because it is more sensitive to semi-central and peripheral collisions, as these will be mainly considered in this work. The correlation between multiplicity and centrality intervals is defined as in experiments in the following way: the lower limit of the highest multiplicity bin, called $PM5$, is fixed at half of the plateau value, and the remaining multiplicity range is divided into four equally spaced intervals, denoted by $PM4$ to $PM1$. $PM5$ then corresponds to most central reactions, and $PM4$ and $PM3$ to semi-central and peripheral ones, respectively [47].

A. Nuclear stopping

We start the flow analysis with the longitudinal distributions which are characterized in terms of the rapidity $Y_{cm} = \frac{1}{2} \ln(1 + \beta_{c.m.}) / (1 - \beta_{c.m.})$. Here the normalised

rapidity $Y^{(0)} = Y_{c.m.} / Y_{c.m.}^{proj}$ is considered.

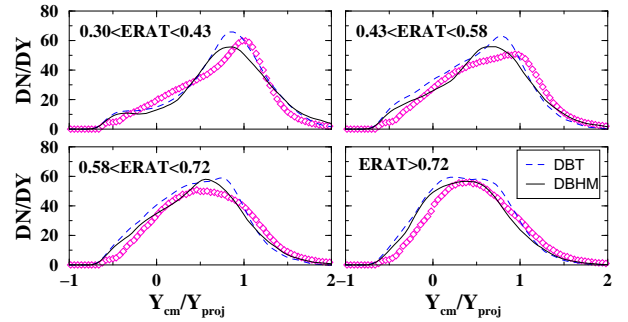


FIG. 9. Rapidity distributions for Au+Au collisions at 0.4 AGeV beam energy. The different centrality intervals run from peripheral (upper left) to central (lower right) collisions. The curves have the same meaning as in the Fig. 7.

The rapidity distributions are shown in Fig.9 for different centrality classes (using the $ERAT$ selection [44]). This observable is strongly affected by detector cuts [44,47], which is reflected in the asymmetry of these distributions relative to the c.m.-rapidity, due to the angular limitations of the FOPI-detector (Phase-I) [47].

It is seen that both models are able to generally reproduce the experimental results. Stopping is most influenced by the NN cross sections, which are the same in both models. There is expected to be an indirect influence from the EOS, because a softer and less momentum dependent EOS leads to more compression and thus to more collisions. However, the differences are not very pronounced which reflects the fact that the EOSs are still similar in the explored density regime and do not differ too much even at the maximal densities reach in such reactions ($\rho \approx 2 - 3 \rho_0$). Only in peripheral collisions, where the deflection of spectator matter by the repulsive momentum dependent component of the mean field plays a more dominant role, the rapidity distributions show differences. Similar trends have been observed in in Ref. [44].

B. In-plane flow

Next we consider the emission of matter projected onto the reaction plane described by the mean in-plane or side-ward flow [5,6]. Fig. 10 compares the mean in-plane proton flow $\langle p_x/A \rangle$ in semi-central ($PM4$) Au+Au collisions at incident energies of 250, 400 and 600 AMeV to the FOPI data from [48]. Both models reproduce the energy dependent increase of the proton flow and are generally in good agreement with the data. We observe that DBHM leads to a stronger in-plane flow in the spectator rapidity region whereas the slope near mid-rapidity $Y^{(0)} \sim 0$ is less affected by the differences in density and momentum dependence of the mean fields. At 600 AMeV DBHM starts to overpredict the slope of the in-plane flow whereas DBT is still in reasonable agreement with exper-

iment. This reflects again the more repulsive character of the DBHM forces which becomes more pronounced with increasing energy, in particular in the spectator region $Y^{(0)} \sim 1$. On the other hand, DBT describes the in-plane flow well around midrapidity but slightly underpredicts it in the spectator region.

The situation is more clearly seen when the mean directed flow P_x^{dir} , i.e. the in-plane flow integrated over the forward hemisphere ($Y^{(0)} \geq 0$), is considered. In Fig.11 the excitation function of P_x^{dir} is shown. As in Fig.10 semi-central (PM4) reactions are considered and compared to the FOPI results [48]. P_x^{dir} is a measure for the overall repulsion experienced by the reaction. Here, as already seen in Fig.10, DBT is in good agreement with experiment at higher energies but underpredicts the flow at lower energies. and for DBHM the situation is just opposite. Due to the FOPI acceptance P_x^{dir} is dominated by the bounce-off of spectator matter at $Y^{(0)} \sim 1$ (see the corresponding rapidity distributions in Fig. 9) which explains the low value of DBT at 0.4 AGeV.

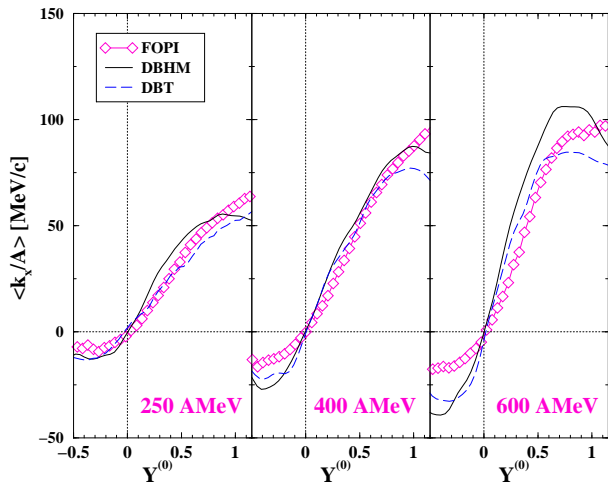


FIG. 10. Mean in-plane transverse flow of protons versus normalised rapidity for semi-central (PM4) Au+Au collisions at 0.25, 0.4 and 0.6 AGeV beam energy. The curves have the same meaning as in Fig. 7. The experimental results are taken from [48].

This behaviour of the in-plane flow results from the interplay of the momentum and density dependence of the self energies (see Figs. 2, 3). The more repulsive character of the DBHM mean fields, in particular at high densities, produces a bounce-off of the spectator remnants in the reaction plane, resulting in too high transverse momenta near spectator rapidities at energies above 0.6 AGeV. This effect is also consistent with the dependence on the relative velocity of the CNM EOS shown in Fig. 6. In the DBT case this is softer at high relative velocities of the counterstreaming currents, i.e. at high bombarding energy. Thus, the comparison of in-plane flow with experiment shows that both microscopic models can explain the experimental results qualitatively. However, they span the range of experimental data of the directed

flow from low to intermediate energies.

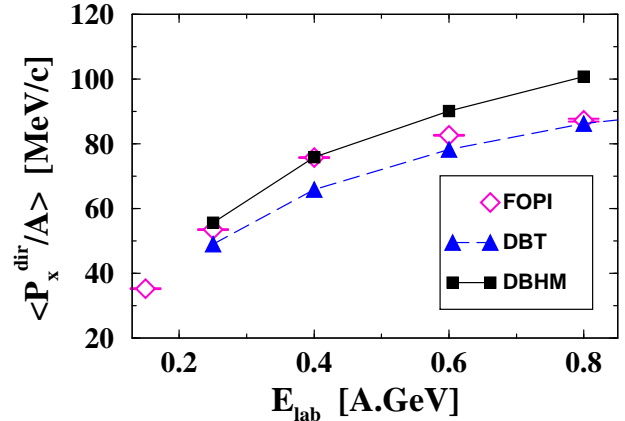


FIG. 11. Excitation function of the mean directed in-plane flow for semi-central (PM4) Au+Au collisions (data from [48]). The curves have the same meaning as in Fig. 3.

As a differential observable the dependence of the in-plane flow on transverse momentum p_t has recently attracted great interest. While to the global properties of the transverse flow, as expressed by P_x^{dir} or $\langle p_x/A \rangle$, give an average over the entire evolution of the collision, the p_t dependence allows to obtain information on different stages of the reaction. High p_t nucleons, but also pions [35], originate from the early and high density phase of the reaction. This is a general feature of heavy ion collisions and seems to hold at bombarding energy from SIS [10] to AGS and SPS energies [49]. In Ref. [9] is was pointed out, in particular, that the p_t dependence of the transverse flow in peripheral reactions is particularly sensitive to the momentum dependence of the nuclear mean field.

The $p_t^{(0)}$ -dependence ($p_t^{(0)} = p_t/p_{c.m.}^{proj}$) of the in-plane flow has been discussed in terms of a Fourier analysis of the experimental azimuthal distribution [50]

$$\frac{dN}{d\phi}(p_t^{(0)}, Y^{(0)}) = v_0(1 + 2v_1 \cos(\phi) + 2v_2 \cos(2\phi)) \quad (9)$$

In Eq. (9) v_0 is a normalisation constant, $v_1(p_t^{(0)}, Y^{(0)})$ describes the in-plane collective flow and $v_2(p_t^{(0)}, Y^{(0)})$ the emission perpendicular to the reaction plane, also called elliptic flow. The quantities $v_{1,2}$ can be determined directly as $v_1 = \langle p_x/p_t \rangle$ and $v_2 = \langle (p_x^2 - p_y^2)/p_t^2 \rangle$, where $p_t = \sqrt{p_x^2 + p_y^2}$ is the transverse momentum per nucleon.

Fig. 12 shows the $p_t^{(0)}$ -dependence of the in-plane flow (v_1) at normalised rapidities $0.5 \leq Y^{(0)} \leq 0.7$ for semi-central (PM4) Au+Au reactions at 0.4 AGeV incident energy for protons ($Z = 1$) and for light fragments ($Z = 2 + 3$).

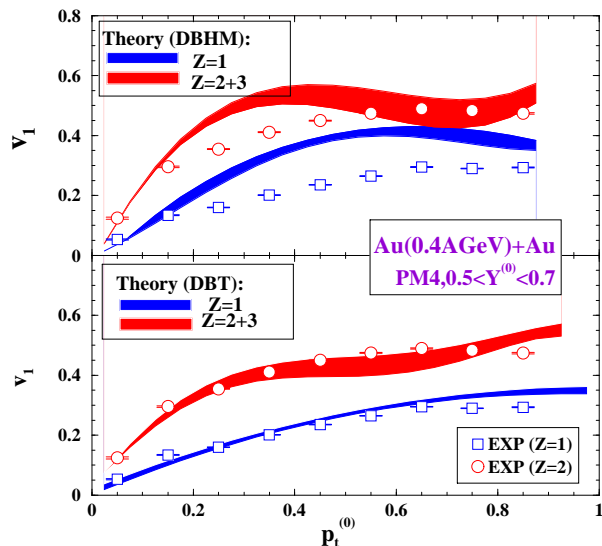


FIG. 12. In-plane flow in terms of the first Fourier coefficient (see Eq. (9)) for semi-central (PM4) Au+Au collisions at 0.4 AGeV for protons and light fragments (preliminary data from [51]). Statistical errors of the calculations are indicated by bands.

A significant model dependence of the differential in-plane flow is observed. At low transverse momenta ($p_t^{(0)} \leq 0.2$) the two models do not show large differences. Since the mean transverse flow is dominated by low p_t particles the $\langle p_x/A \rangle$ observable therefore does not differentiate between the two models in the present situation. Consequently, in Fig.10 the two curves for $\langle p_x/A \rangle$ (0.4 AGeV) lie almost on top of each other in the considered rapidity range. However, the difference between the models becomes pronounced when higher transverse momenta ($p_t^{(0)} \geq 0.2$) are studied. In Fig. 12 DBT reproduces the data very well for both, protons and light fragments, whereas DBHM overpredicts the flow significantly which reflects its more repulsive character at baryon densities above ρ_0 . The comparison to data favours a weaker repulsion at higher densities as predicted by DBT. In contrast to the global P_x^{dir} observable the quantity $v_1(p_t^{(0)}, Y^{(0)})$ is more sensitive to high density matter in the participant region.

The situation is similar for light fragments ($Z = 2 + 3$) which, however, show a stronger collectivity compared to free nucleons, as also seen in Fig.12. This can be understood by assuming that the heavier fragments are mainly formed in the spectator regions, whereas the free nucleons cover the entire phase space. Thus, one obtains on the average a higher mean transverse momentum $\langle p_x/A \rangle$ for fragments than for nucleons. This scenario of the fragment formation is consistent with the findings in Ref. [46] that the spectator enters into an instability region with conditions which are near the experimental ones for a liquid-gas phase transition [52].

C. Out-of-plane flows

A preferential out-of-plane emission of particles, the so-called squeeze-out, is characterised by negative values of the second Fourier coefficient v_2 in Eq. (9) whereas a positive value of v_2 indicates in-plane flow [50]. A related variable to characterise the azimuthal anisotropy of particle emission is the squeeze-out ratio R_N defined by $R_N = (N(\Phi = 90^\circ) + N(\Phi = 270^\circ))/(N(\Phi = 0^\circ) + N(\Phi = 180^\circ)) = (1 - 2v_2)/(1 + 2v_2)$ [54]. In terms of R_N an isotropic emission corresponds to $R_N = 1$, $R_N > 1$ indicates squeeze-out and $R_N < 1$ a preferential in-plane emission. At lower energies squeeze-out is mainly due to shadowing of the participant particles by the spectators and it is therefore most pronounced for mid-rapidity particles.

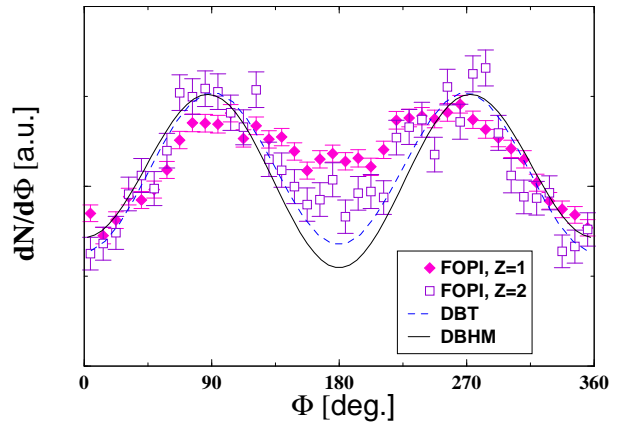


FIG. 13. Azimuthal distributions at mid-rapidity ($|\Delta Y^{(0)}| \leq 0.15$) for semi-central Au+Au collisions at 0.6 AGeV beam energy (data from [55]).

Fig. 13 shows the azimuthal distributions at mid-rapidity for all charged particles (nucleons plus fragments) in semi-central Au+Au collisions at 0.6 AGeV. The calculations are compared to experimental results from FOPI [55] for $Z = 1$ and $Z = 2$ fragments. The data show a stronger out-of-plane emission for $Z = 2$ fragments relative to those for nucleons which is due to the higher collectivity of fragments as discussed above. Due to limited statistics the theoretical values in Fig. 13 are given for all charged particles. We observe a qualitatively good agreement between theory and experiments, although both calculations slightly overestimate the data. In line with the discussion of the in-plane flow we obtain a stronger out-of-plane emission of participant matter using the DBHM forces due to the stronger repulsive mean field at high densities.

A more sensitive way to probe the momentum dependence of the mean field is the transverse momentum dependence of the elliptic flow v_2 . This is shown in Fig. 14 for peripheral Au+Au collisions (PM3 multiplicity interval, $b_{\text{mean}} \sim 7\text{fm}$) at 0.4 AGeV. Consistent with the picture that squeeze-out is mainly due to shadowing which

is most effective in the early high density phase of the reaction the elliptic flow becomes increasingly negative with increasing p_t . As already mentioned high p_t particles probe the high density phase of the reaction. Using the DBHM forces the p_t dependence of the squeeze-out is much more steep than for DBT, which on the other hand, is closer to the data of [45].

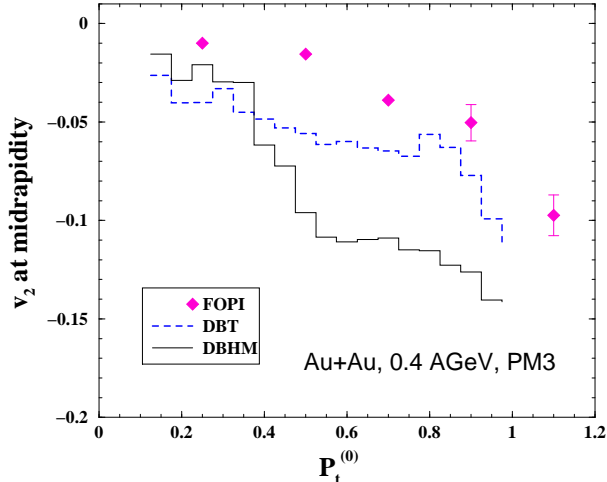


FIG. 14. Transverse momentum dependence of the elliptic flow at midrapidity ($|\Delta Y^{(0)}| \leq 0.1$) v_2 for peripheral (PM3) Au+Au collisions at 0.4 AGeV. Data are taken from [45].

This behaviour is also consistent with the findings of Ref. [45] where soft and hard Skyrme forces within the framework of the QMD model were subjected to a comparison of the same observable. The softer equations-of-state (soft Skyrme in [45] and DBT in the present case) yield a slower increase of v_2 and are in reasonable agreement with experiment. However, in Ref. [45] both version of Skyrme forces have an identical momentum dependence whereas in the present case DBHM is significantly more repulsive. In the analysis of Ref. [10], on the other hand, Skyrme parameterisations were used which show the same density dependence, i.e. the same EOS, but differed in their momentum dependence. A stronger repulsive character of the model, expressed by both, a stiffer EOS and/or a stronger momentum dependence generally results in a stronger squeeze-out signal for high p_t particles. Hence, it is difficult to disentangle these two sources of the squeeze-out. The authors of Ref. [10] favour a parameterisation (HM in Ref. [10]) which yields results for this observable close to DBHM in our case. The comparison to the most recent FOPI data [45], shown here in Fig. 14, might change the conclusions drawn in Ref. [10].

In Fig.15 the same analysis is performed for the $Ru + Ru$ system. Here the differential components of the in-plane and out-of plane flow in terms of the Fourier-coefficients v_1 and v_2 as a function of the transverse momentum and rapidity are shown. The rapidity intervals are $-0.7 < Y^{(0)} < -0.5$ and $-0.3 < Y^{(0)} < -0.1$ for the

v_1 and v_2 analysis, respectively. Both, DBHM and DBT are in fair agreement with the FOPI data [27] on the v_2 observable. However, the p_t dependence of the in-plane flow v_1 strongly depends on the model. As already observed for the $Au + Au$ system (Fig.12) DBHM strongly overpredicts the flow v_1 at intermediate p_t . We summarize our findings in the following way: The differences observed in the v_1 observable are due to the different momentum dependence of the fields. The v_2 observable shows much less model dependence. In the smaller system the compressional effects are smaller which reduced the sensitivity to the different momentum dependence.

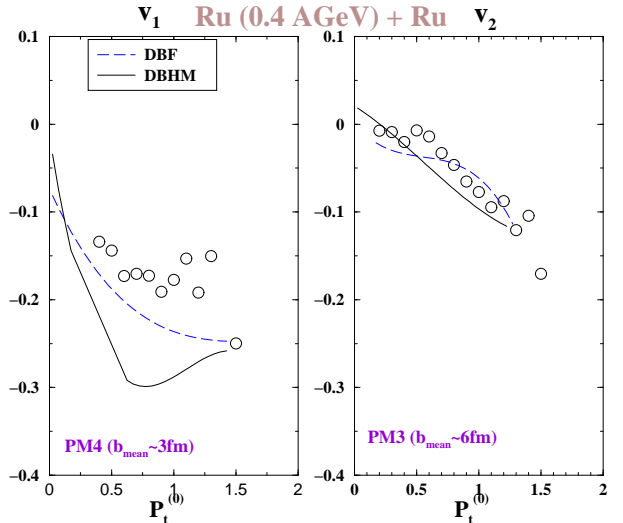


FIG. 15. Transverse momentum dependence of the first (v_1 , left) and second (v_2 , right) azimuthal flow Fourier-coefficients for the system $Ru+Ru$ at 0.4 AGeV incident energy extracted in rapidity intervals of $-0.7 < Y^{(0)} < -0.5$ (left) and $-0.3 < Y^{(0)} < -0.1$ (right) for semi-central (PM4) and peripheral (PM3) reactions, respectively (data from [27]).

In Fig. 16 the centrality dependence of the squeeze-out ratio R_N at midrapidity ($|\Delta Y^{(0)}| < 0.15$) for particles with high transverse momenta ($0.4 < p_t^{(0)} < 0.55$) is shown. The decrease of the squeeze-out ratio R_N at higher impact parameters can be explained by the strong vector repulsion of the nuclear mean field. Again both models can reproduce the centrality dependence of the experimental data qualitatively, but not in detail. The DBHM calculations overpredict the data at low impact parameters, whereas DBT underpredicts the data for peripheral collisions. Similar results have been found in recent studies of the FOPI collaboration in comparison with the IQMD model with phenomenological Skyrme-parametrisations with a soft/hard EOS [27].

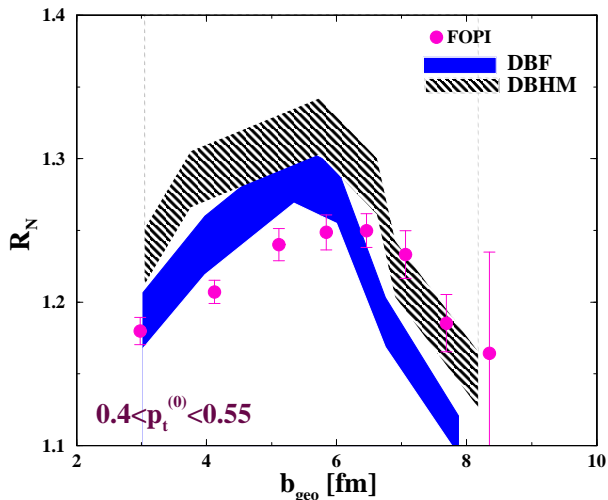


FIG. 16. Centrality dependence of the squeeze-out ratio R_N at mid-rapidity ($|\Delta Y^{(0)}| < 0.15$) for Au+Au collisions at 0.4 AGeV (data from [55]). Statistical errors of the calculations are indicated by bands.

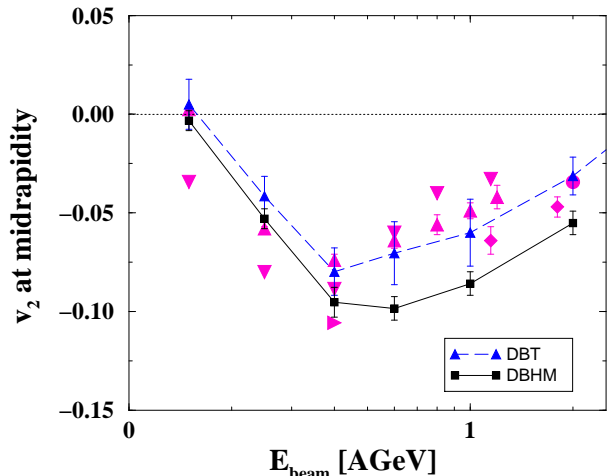


FIG. 17. Energy dependence of the elliptic flow v_2 at mid-rapidity. The data are taken from the FOPI- (triangles) [45], EOS (diamonds) [56], Plastic Ball (triangles down) [6], LAND (triangle right) [6] and E895 (circle) [56].

Finally, Fig.17 shows the excitation function of the elliptic flow v_2 . With increasing beam energy a considerable emission perpendicular to the reaction plane can be seen ($v_2 < 0$) which approaches a maximum around 0.4 AGeV and then decreases again. This behaviour can be understood by shadowing and compression effects as discussed in detail in Ref. [56]. Again both models reproduce the general trend of a sample of experimental data shown in Fig.17. However, with DBHM the maximum of negative v_2 values is slightly shifted to higher energies and the absolute values are larger. The experimental data which are a sample of available data from FOPI [45], EOS [56], Plastic Ball [6], LAND [6] and E895

[56] show strong variations in magnitude of the v_2 coefficient which cover the range of the theoretical calculations. However, DBT better reproduces the maximum at the correct energy and lies closer in absolute magnitude to the most recent data from FOPI [45]. Assuming that the latter are the most reliable measurements, e.g. with respect to reaction plane corrections etc., the comparison to experiment favours the DBT mean fields.

VI. SUMMARY

We investigated the collective nucleon flow in heavy ion collisions at intermediate energies (0.15 ÷ 1 AGeV) within a relativistic BUU transport model with mean fields based on relativistic Dirac-Brueckner-Hartree-Fock (DB) calculations for nuclear matter. The anisotropy of the local momentum space in the participant region of heavy ion reactions was taken into account in the colliding nuclear matter approximation. The main effect of this is a softening of the effective EOS seen by the particles in the colliding system.

We compared two different DB predictions, those of ter Haar and Malfliet (DBHM) and the more recent calculations performed by the Tübingen group (DBT). From a theoretical point of view the latter ones have a stronger physical foundation since spurious contributions from a strong coupling of a pseudo-scalar πNN vertex to negative energy states were removed by an improved projection scheme for the in-medium T-matrix. Compared to DBHM the corresponding EOS is slightly softer ($K=250/230$ MeV for DBHM/DBT) and the effective mass is significantly larger ($m^* = 558/637$ MeV for DBHM/DBT). This results in smaller fields and a less repulsive optical potential for DBT. The smaller repulsion of the DBT model is also expressed in terms of a larger non-local effective mass ($m_{NR}^* = 0.63/0.73 M$ for DBHM/DBT) which is commonly used in non-relativistic approaches in order to classify the strength of the momentum dependence of the potential.

Both models yield a reasonable description of in-plane and out-of-plane flow observables. A more detailed comparison to data, in particular the transverse momentum dependence of v_1 and v_2 favours the softer EOS and the less repulsive character of the DBT predictions at the higher energies. At 0.6 and 0.8 AGeV DBT also yields a very accurate description of the transverse in-plane flow whereas at lower energies the in-plane flow requires some more repulsion as provided by the DBHM model. Interestingly, a similar observation was made in the non-relativistic approach of Ref. [10]. In summary, the microscopic DB approach, where no parameters are adjusted to the nuclear matter saturation properties nor to the empirical optical nucleon-nucleus potential, predicts a density and momentum dependence of the mean field which to a large extent is consistent with the observations from heavy ion collisions.

ACKNOWLEDGMENTS

We are grateful to A. Andronic from FOPI for many discussions concerning the interpretation of data.

-
- [1] E.A. Uehling, G.E. Uhlenbeck, Phys. Rev. **43** (1933) 552; P. Danielewicz, Ann. Phys. **152** (1984) 239; G.F. Bertsch, S. Das Gupta, Phys. Rep. **160** (1988) 189.
- [2] B. Blättel, V. Koch, U. Mosel, Rep. Prog. Phys. **56** (1993) 1.
- [3] S. Hama, B.C. Clark, E.D. Cooper, H.S. Sherif, R.L. Mercer, Phys. Rev. **C41** (1990) 2737; E.D. Cooper, S. Hama, B.C. Clark, R.L. Mercer, Phys. Rev. **C47** (1993) 297.
- [4] J. Aichelin, H. Stöcker, Phys. Lett. **B176** (1986) 14.
- [5] W. Reisdorf and H.G. Ritter, Annu. Rev. Nucl. Part. Sci. **47** (1997) 663.
- [6] N. Herrmann, J.P. Wessels, T. Wienold, Annu. Rev. Nucl. Part. Sci. **49** (1999) 581, and refs. therein.
- [7] P.K. Sahu, A. Hombach, W. Cassing, M. Effenberger, U. Mosel, Nucl. Phys. **A640** (1998) 493; A. Hombach, W. Cassing, S. Teis, U. Mosel, Eur. Phys. J. **A5** (1999) 157.
- [8] P.K. Sahu, W. Cassing, U. Mosel, A. Ohnishi, Nucl. Phys. **A672** (2000) 376.
- [9] P. Danielewicz, Nucl. Phys. **A673** (2000) 375.
- [10] A.B. Larionov, W. Cassing, C. Greiner, U. Mosel, preprint nucl-th/0006009.
- [11] C. Fuchs, T. Gaitanos, H.H. Wolter, Phys. Lett. **B381** (1996) 23.
- [12] T. Gaitanos, C. Fuchs, H.H. Wolter, Nucl. Phys. **A650** (1999) 97.
- [13] B. D. Serot, J. D. Walecka, Advances in Nuclear Physics, **16**, 1, eds. J. W. Negele, E. Vogt, (Plenum, N.Y., 1986)
- [14] P. Ring, Prog. Part. Nucl. Phys. **78** (1996) 193.
- [15] F. Weber, J. Phys. **G25** (1999) R195.
- [16] B. D. Serot and J. D. Walecka, *Int. J. Mod. Phys. E* **6** (1997) 515.
- [17] R.J. Furnstahl, B.D. Serot, and H.-B. Tang, *Nucl. Phys.* **A615**, 441 (1997); H.W. Hammer, R.J. Furnstahl, *Nucl. Phys.* **A678**, 272 (2000).
- [18] M. Lutz, B. Friman, Ch. Appel, Phys. Lett. **B474** (2000) 7.
- [19] G.J. Horowitz, B.D. Serot, Phys. Lett. **B137** (1984) 287; Nucl. Phys. **A464** (1987) 613.
- [20] W. Botermans, R. Malfliet, Phys. Reports **198** (1990) 115.
- [21] B. ter Haar, R. Malfliet, Phys. Reports **149** (1987) 207.
- [22] C. Fuchs, T. Waindzocho, A. Faessler, D.S. Kosov, Phys. Rev. **C58** (1998) 2022.
- [23] T. Gross-Boelting, C. Fuchs, A. Faessler, Nucl. Phys. **A648** (1999) 105.
- [24] C. Fuchs, H. Lenske, H.H. Wolter, Phys. Rev. **C52** (1995) 3043.
- [25] R. Machleidt, *The Meson Theories of Nuclear Forces and Nuclear Structure*, Advances in Nuclear Physics **19** (1989) 189.
- [26] C. Fuchs, E. Lehmann, L. Sehn, F. Scholz, J. Zipprich, T. Kubo, and Amand Faessler, Nucl. Phys. **A603** (1996) 471.
- [27] N. Bastid (FOPI collaboration), *Structure of the Nucleus at the Dawn of the Century*, (Publisher, Bologna 2000) XXX.
- [28] C. Fuchs, P. Essler, T. Gaitanos, H.H. Wolter, Nucl. Phys. **A626** (1997) 987.
- [29] R.K. Puri, N. Ohtsuka, E. Lehmann, A. Faessler, H.M. Martin, D.T. Khoa, G. Batko, and S.W. Huang, Nucl. Phys. **A536** (1992) 201.
- [30] L. Sehn, H.H. Wolter, Nucl. Phys. **A601** (1996) 473.
- [31] D.T. Khoa, N. Ohtsuka, M.A. Matin, A. Faessler, S.W. Huang, E. Lehmann, R.K. Puri, Nucl. Phys. **A548** (1992) 102.
- [32] C. Fuchs, T. Gaitanos, to be published.
- [33] S. Huber and J. Aichelin, Nucl. Phys. **A573** (1994) 587.
- [34] Ch. Hartnack, R.K. Puri, J. Aichelin, J. Konopka, S.A. Bass, H. Stöcker, W. Greiner, Eur. Phys. J. **A1** (1998) 151.
- [35] V.S. Uma Maheswari, C. Fuchs, Amand Faessler, L. Sehn, D. Kosov, Z. Wang, Nucl. Phys. **A628** (1998) 669.
- [36] C. Fuchs, H.H. Wolter, Nucl. Phys. **A589** (1995) 732.
- [37] H. Sorge, H. Stöcker, W. Greiner, Ann. Phys. **192** (1989) 266.
- [38] N. Ohtsuka, R. Linden, A. Faessler, F.B. Malik, Nucl. Phys. **A465** (1987) 550; I. Izumoto, S. Krewald, A. Faessler, Nucl. Phys. **A341** (1980) 319;
- [39] M. Baldo, I Bombaci, G. Giansiracusa, and U. Lombardo, Phys. Rev. **C40** (1989) R491.
- [40] W. Zuo, I. Bombaci, U. Lombardo, Phys. Rev. **C60** (1999) 024605.
- [41] F. de Jong and H. Lenske, Phys. Rev. **C54** (1996) 1488.
- [42] G.Q. Li and R. Machleidt, Phys. Rev. **C48** (1993) 2707.
- [43] S. Typel, H.H. Wolter, to be published.
- [44] V. Ramillien (FOPI-Collaboration), Nucl. Phys. **A587** (1995) 802.
- [45] A. Andronic *et al.* (FOPI collaboration), Nucl. Phys. **A661** (1999) 333c.
- [46] T. Gaitanos, H.H. Wolter, C. Fuchs, Phys. Lett. **B478** (2000) 79.
- [47] W. Reisdorf (FOPI-Collaboration), Nucl. Phys. **A612** (1997) 493.
- [48] F. Rami *et al.* (FOPI Collaboration), Nucl. Phys. **A646** (1999) 367.
- [49] E. Zabrodin, C. Fuchs, L.V. Bravina, A. Faessler, nucl-th/0006056, Phys. Rev. **C** in press.
- [50] A. M. Poskanzer and S. A. Voloshin, Phys. Rev. **C58** 1671 (1998) 1671.
- [51] A. Andronic, private communication. Note that the data shown in Fig. 12 are preliminary and may still shifted upwards by about 10%.
- [52] T. Odeh *et al.* (ALADIN Collaboration), Phys. Rev. Lett. **84** (2000) 4557.
- [53] F. Daffin, K. Haglin, and W. Bauer, Phys. Rev. **C54** (1996) 1375.
- [54] P. Crochet *et al.* (FOPI-Collaboration), Nucl. Phys. **A624** (1997) 755.

- [55] P. Crochet (FOPI-Collaboration), *XXXIV International Winter Meeting of Nuclear Physics* (I. Iori, Bormio 1996); N. Bastid *et al.* (FOPI-Collaboration), Nucl. Phys. **A622** (1997) 573.
- [56] C. Pinkenburg *et al.* , Phys. Rev. Lett. **83** (1999) 1295; P. Danielewicz, Roy A. Lacey, *et al.* , Phys. Rev. Lett. **81** (1998) 2438.